Half-Time 4 months
May 2019

MAGNETIC CHARACTERIZATION OF SELF-ASSEMBLED ONE-DIMENSIONAL NETWORKS OF MAGNETIC NANOPARTICLES

Mario Salvador López Muñoz

Bachelor thesis supervised by Rasmus Westerström

Division of Synchrotron Radiation
Department of Physics
Faculty of Natural Science

LUND
UNIVERSITY

Abstract

In this thesis, a magnetic study of two different arrangements of Fe_3O_4 nanoparticles is presented. The nanoparticles are generated using an aerosol technique and guided onto a substrate. The first sample was produced by guiding the nanoparticles onto the substrate using an electric field, resulting in large clusters of randomly oriented Nanoparticle (NP). The second sample was created by also applying a magnetic field which resulted in the formation of self-assembled networks of one-dimensional Nanowire (NW) made up from individual nanoparticles. To measure the magnetic properties of the samples a Superconduntin Quantum Interference Device (SQUID) is used. Magnetization curves measured at 300 K and 1.8 K show a difference in the magnetization behavior for the two samples and an increase in the remanent magnetization of 50% for the self-assembled structures. The results are interpreted based on the Stoner-Wohlfarth model, and the shortcomings of applying this model to our systems are discussed.

Contents

Acronyms

DMA Differential Mobility Analyzer.

MD Multi Domain.

NP Nanoparticle.

NW Nanowire.

SD Single Domain.

SDG Spark Discharge Generation.

SPM Super-paramagnetism.

SQUID Supercondunting Quantum Interference Device.

SW Stoner-Wohlfarth.

1 Introduction

The following project is a Bachelor thesis on the area of Nanomagnetism where self-assembled structures of magnetite (Fe_3O_4) nanoparticles are studied. Magnetic self-assembled structures made up of nanoparticles could be used in catalysis [1], energy storage [2], Micro [3] and Gigahertz [4] absorption, and as building blocks for future high performing permanent magnets [5]. For this project, the structures are created using an aerosol technique based on a Spark Discharge Generation (SDG) capable of producing particles with tunable composition, crystal structure, and narrow size distribution that can be deposited onto any substrate. The versatility of the technique provides the means for generating magnetic nanostructures where the building blocks could be tailored for a specific application. The project will compare two samples created using the same technique, one made up from large clusters of nanoparticles (fig. 1 (a)) and another with the nanowires structure (fig. 1 (b)-(d)). From now on I will refer to the two systems with the abbreviated form of NP and NW respectively. The goal of the project is to see if there is any difference in the magnetic response due to the formation of the nanowire structures. The magnetic measurements are performed using a Supercondunting Quantum Interference Device (SQUID) magnetometer. Magnetization curves from the two samples reveal a difference in the initial magnetization behavior and an increase of the remanent magnetization for the NW sample. The differences between the samples obtained are interpreted using the Stoner-Wohlfarth model [6], and the shortcomings of applying this model to our systems are discussed.

This Bachelor thesis is a part of a larger project that is studying how the particle size, particle composition, and deposition parameters determine the self-assembly. The long term goal is to produce well defined self-assembled structures of different materials that can be guided using, e.g., lithography or magnetic nanostructures. This project is in its starting phase, and the results presented in this thesis are the first magnetic measurements performed on the self-assembled structures.

The first section after the introduction consists of a theoretical background and summary with some important concepts from magnetism, nanoparticles, and anisotropy. The second section will describe the technique and the devices used to create and characterize the sample. The following section will consist of a presentation and interpretation of the results. And the last will be a conclusion. The appendices attached describe the handling of the samples, the data treatment.

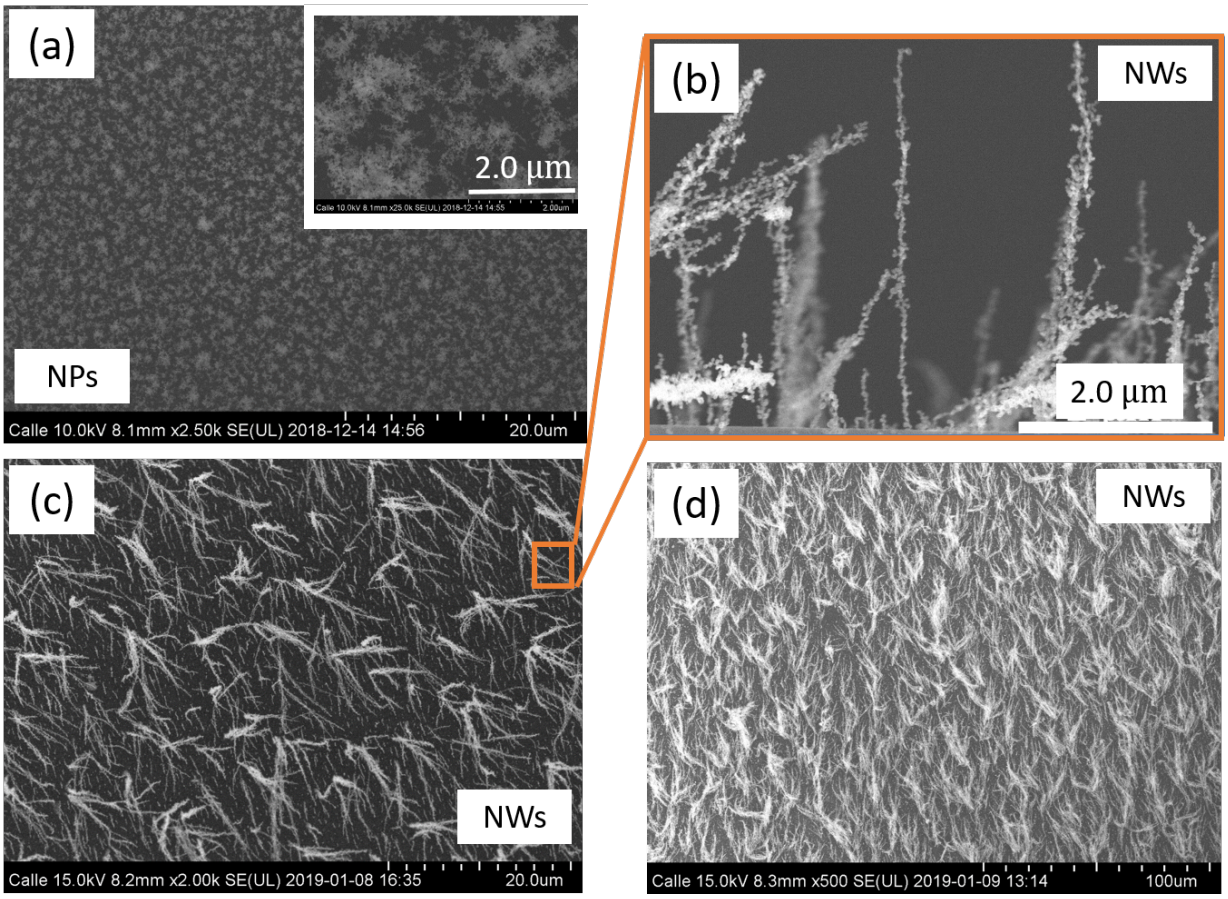

Figure 1: Images recorded using a scanning electron microscope showing large clusters of nanoparticles (a) and self-assembled structures made up of one-dimensional nanowires (b)-(d).

2 Theory

2.1 Magnetic Dipoles

It is essential first to explain some key concepts to understand the following project. It is important to know that a magnetic field is generated by magnetic moments. A magnetic moment is a quantity that represents the magnetic strength of an object and a magnetic dipole has a magnetic moment that is directed from the magnetic south pole to the magnetic north pole. As can be seen in the following picture:

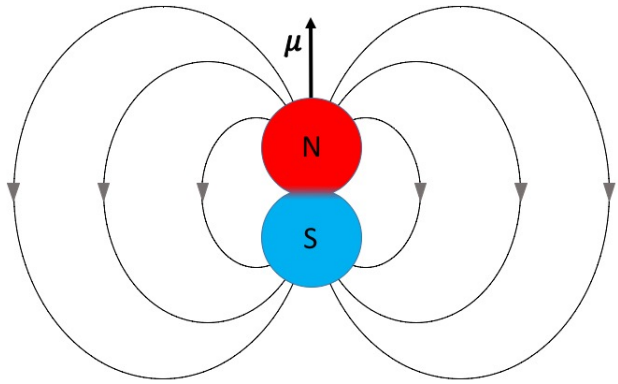

Figure 2: Magnetic moment $\boldsymbol{\mu}$ of a dipole and magnetic field lines

Likewise, a magnetic dipole in a magnetic field experiences a torque, $\boldsymbol{\tau} = \boldsymbol{\mu} \times \boldsymbol{B}$ and wants to align with the field. Like a compass needle in the earth's magnetic field. The potential energy of such interaction is:

$$U = -\boldsymbol{\mu} \cdot \boldsymbol{B} = -\mu B cos\theta \tag{2.1}$$

Where θ is the angle between the moment $\boldsymbol{\mu}$ and the magnetic field $\boldsymbol{B}$. This way, a magnetic field created by a dipole can affect nearby dipoles, in what is called dipole-dipole interaction.

2.2 The Magnetic Moment

At this point, it is reasonable to wonder about the nature of this phenomena. The electron orbiting around the nucleus originates microscopic loop currents and an orbital moment. Using the semi-classical picture, similar to a loop of current generates a magnetic moment, an electron bound to a nucleus can generate a magnetic moment corresponding to the angular momentum of the electron.

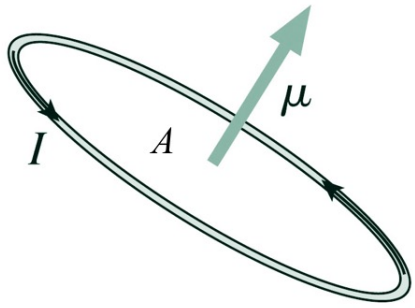

Figure 3: Magnetic moment $\boldsymbol{\mu}$ of a loop of area A with current I

The magnetic moment of the electron orbiting around the nucleus in an atom can be written as:

$$\mu_L = m_L \mu_B \tag{2.2}$$

Where m_L is the orbital magnetic quantum number

Besides orbiting around the nucleus, the electron has an intrinsic angular moment which adds to the magnetic moment; this is the spin. The spin magnetic moment is described by:

$$\mu_S = g_S m_S \mu_B \tag{2.3}$$

Here, $g_S = 2$. The spin magnetic moment interacts with the magnetic field generated by the orbital angular moment. The interaction between spin and orbit gives birth to the spin-orbit coupling. The total angular momentum, J, is defined as J=L+S, where L and S are the total orbital and spin angular moment from the valence electrons. With this the magnetic moment becomes:

$$\mu_J = g_J m_J \mu_B \tag{2.4}$$

Where

$$g_J = \frac{3}{2} + \frac{S(S+1) - L(L+1)}{2J(J+1)} \tag{2.5}$$

Just as a macroscopic dipole moment interacts with an external field as the compass needle in the earth's magnetic field, the atomic magnetic moments will also interact with an external field. This is called the Zeeman interaction.

$$E_Z = -\boldsymbol{\mu_J} \cdot \boldsymbol{B} = -g_J m_J \mu_B B \tag{2.6}$$

2.3 Magnetization

When materials with magnetic moment are in the presence of an external magnetic field, they can be magnetized. The relation between magnetization and the external magnetic field is :

$$\mu_0 \boldsymbol{M} = \chi_m(T) \boldsymbol{B} \tag{2.7}$$

Where χ_m is the magnetic susceptibility of the material as a function of the temperature, and the magnetization, $\boldsymbol{M}$, is the dipole moment per unit volume. The magnetization can be positive or negative. When it is positive, we call that material paramagnetic, and when it is negative, it is called diamagnetic. Paramagnetic materials align their magnetic field parallel to the external magnetic field while diamagnetic align it anti-parallel. All materials present a diamagnetic response which can result in interesting effects, like magnetic levitation [7]. Paramagnetism is due to the Zeeman effect. A purely paramagnetic moment interacts with a magnetic field but not with neighboring atoms. It only occurs for atoms with incomplete shells since unpaired electrons have a magnetic dipole moment. It is energetically favorable for the atomic magnetic moments to align with the external magnetic field. Opposing the alignment is the thermal energies. In the absence of an applied field and inter-atomic interactions, there is no preferential orientation of the atomic moments, and thus the system is no longer magnetized. The magnetic moments can interact with each other which leads to magnetic ordering. Depending on how the different atoms couple to each other, aligning parallel or anti-parallel, the material is ferromagnetic, anti-ferromagnetic or ferrimagnetic. This effect due to the exchange interaction, which arises from an energy exchange between neighbor spins, [8].

The difference between Ferro- and anti-ferromagnetic materials lies in how moments on different lattice sites orient with respect to each other. For a ferromagnet, neighboring spins tend to align parallel to each other, and in anti-ferromagnetic materials, they align antiparallel, see fig. 4. When the sublattices have the same magnetic moments, then the total magnetization is zero, but when the magnetic moments are unequal, which can happen if they are different materials or if they are different ions, then there's a partial cancellation, and there's a non-zero magnetization. In this case, the material is named ferrimagnetic. Ferrimagnetism is the case of Magnetite, which is composed of two sublattices of Fe^{2+} and Fe^{3+}.

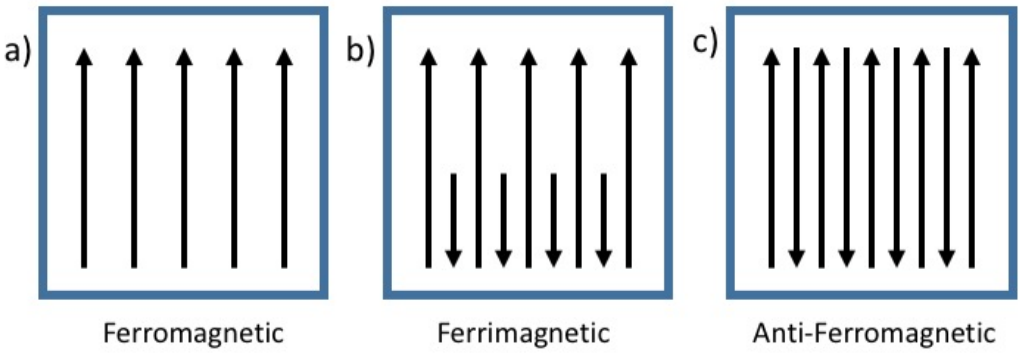

Figure 4: Image showing the magnetization of the different materials with arrows showing the magnetization direction of the sublattices: a)ferromagnetic, b) Ferrimagetic and c) Anti-ferromagnetic.

Magnetization curves relate the magnetization of a magnetic sample with an external, applied magnetic field. For permanent magnets, the magnetization depends on the history of the applied magnetic field and the magnetization curve exhibits hysteresis. Key elements of this curve are: the saturation magnetization, M_s, which is the maximum magnetization possible for the sample; remanent magnetization, M_r, which refers to the magnetization that remains present once the applied magnetic field becomes zero after having some value; coercive field, B_c, which is the external field necessary for the sample to become demagnetized and virgin curve, which is the path that the magnetization follows when starting from a demagnetized state and applying an external field.

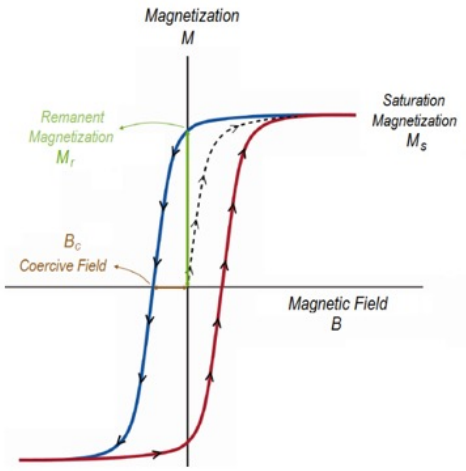

Figure 5: Hystereis diagram, adapted from [9].

The coercive field determines if a magnetic material is soft or hard, soft or hard refer to the resistance that a material has to a change in its magnetized state, this change can be influenced by the external field or by the course of time. Fe_3O_4 is a soft magnet. So it needs a relatively low coercive field to magnetized, and therefore it is easily demagnetized.

2.4 Magnetic Anisotropy

Magnetic anisotropy refers to the existence of crystallographic directions along which it is energetically favorable to orient the magnetic moments. The direction with lowest energy is called magnetic easy-axis. The primary source of anisotropy is usually magnetocrystalline anisotropy. The sample can also have shape and surface anisotropy. The surface could contribute to the anisotropy for systems with a large surface to volume ratio such as NPs. However, it is expected that the differences between the two samples will come from the alignment of the nanoparticles in the NW sample and we are, therefore, here only considering the magnetocrystalline contribution. The magnetocrystalline anisotropy is due to the anisotropic charge distribution of the d-orbitals giving rise to the orbital magnetic moment (see fig. 6). Depending on the symmetry of the crystal field, certain d-orbitals will have lower energy than the others. This means that also the orbital magnetic moments will have crystallographic directions which are energetically favorable. The spin-orbit interaction then couples the spin to the orbital magnetic moment and gives rise to the magnetocrystalline anisotropy.

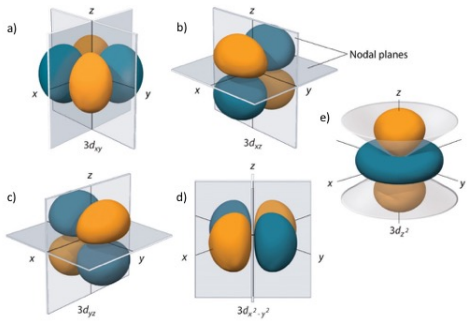

Figure 6: Charge distribution of the 3d orbitals. Adopted from [10].

The most simple case is uni-axial magnetic anisotropy, where the magnetic moments have one magnetic easy axis. The anisotropy energy per unit volume is given by:

$$\frac{E_a}{V} = K_U sin^2(\theta) \tag{2.8}$$

Where K_U is the effective uni-axial anisotropy constant with units energy per unit volume and θ is the angle with respect to the easy-axis. Reversing the magnetic moment is thus associated with an energy barrier proportional to its volume; this function is shown in figure 7 [11]. The anisotropy energy has a is minimum at $\theta = 0$ and $\theta = \pi$ for (K$>$ 0). The system's total energy has a minimum when the external field is parallel to the easy axis. Since the magnetization has the same direction and occurs due to the external magnetic field, the system will be easily magnetized for a magnetic field parallel to the magnetization and the easy-axis.

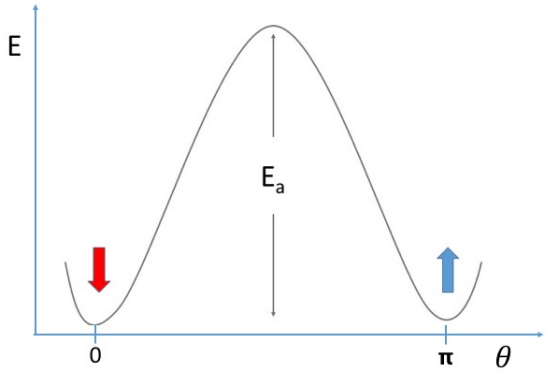

Figure 7: Figure of the anisotropy energy when no external magnetic field is applied, showing the two energy minima, labelled as "up" and "down". The vertical axis represents energy and the horizontal the angle.

As illustrated in fig. 8 the Stoner-Wohlfarth (SW) model takes magnetic particles as homogeneous Single Domain (SD) with the shape of elongated ellipsoids and assumes uniaxial anisotropy. The model considers two components for the energy, the anisotropy, and the Zeeman energy. The total energy of the system at 0 K will be:

$$E_{tot} = E_a + E_Z = K_U \sin^2(\theta) - M_{sat} B \cos(\theta - \phi) \tag{2.9}$$

where eq. (2.8) and eq. (2.6) were used, M_{sat} is the saturation magnetization.

The Stoner-Wohlfarth model[6] can be used to calculate the hysteresis curves for a specific orientation (ϕ) of the external magnetic field (B) with respect to the magnetic easy-axis. If the magnetic easy-axis is aligned with the external field ($\phi = 0$), the SW model predicts that the ratio of the remanent and saturated magnetization is $M_r/M_{sat} = 1$. If instead there is a random orientation of the easy-axis with respect to the external field, as would be the case of the NP sample, the SW model gives a reduction in the remanent magnetization with a factor one-half $M_r/M_{sat} = 1/2$. If the formation of the NWs results in an alignment of the easy-axis, we could expect to see a difference in the ratio M_r/M_{sat} between the two samples.

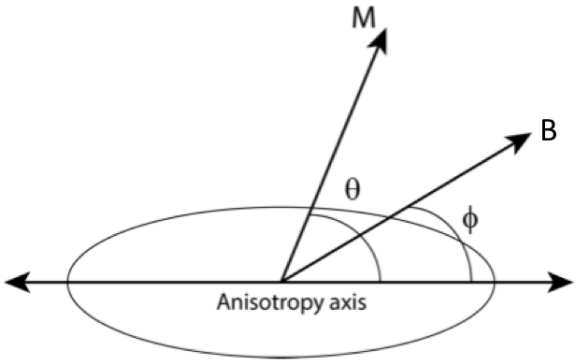

Figure 8: Drawing of a 2D elliptical particle with the magnetization (M) and applied field (B) vectors and their angles(θ and ϕ respectively) with respect to the anisotropy axis as used in the Stoner Wohlfarth model.

2.5 Domains

The size of the particle also has great importance for its magnetic properties. For small sizes, the magnetization of the nanoparticle is oriented along one direction. This is referred to as single-domain, see fig. 10. Particles smaller than the critical diameter, D_{cr}^{spm}, will spontaneously change their magnetization when the thermal energy is of the same order of magnitude than their anisotropy energy $K_BT \sim E_a$. Under these conditions, the moments do not have a preferred orientation in the absence of an external field and thus no hysteresis or coercive field, see fig. 9. This state is referred to as a Super-paramagnetism (SPM) state.

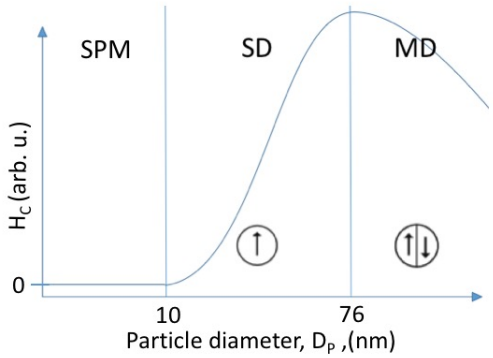

Figure 9: Figure showing the relation between coercive field H_c and the diameter of a particle resulting in 3 regimes: a) superparamagnetism (SPM), b) single domain, c) multi-domain (MD). The arrow shows the direction of the easy-axis for each domain. Values obtained from [12] show the critical sized of Fe_3O_4.

After increasing the size of the particles past the SPM regime, the system remains single-domain but has now enough anisotropy energy to stabilize the magnetization. Consequently, with increasing size, the coercive field also increases up to a critical diameter (SD regime in fig. 9). In the SD, the magnetic moments of the different atoms add up to created one large magnetic moment that can take two directions "up" and "down" and is often referred to as a superspin or macrospin. If the size is further increased, the system will split up into MD, each with its magnetic moment in a different direction (see fig. 10).

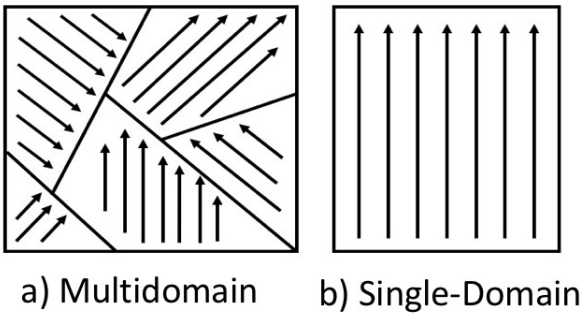

Figure 10: MD and SD illustration, arrow represent the direction of the magnetization for each domain.

Our Nanoparticles are around 50 nm. According to fig. 9, the nanoparticles should be larger than the critical diameter for SPM but still being single-domain. Even if it's not super-paramagnetic, our system will be more affected by thermal energies than if it were closer to the maximum value of the function, the critical size for SD.

2.6 Fe_3O_4 and cubic anisotropy

Magnetite(Fe_3O_4) is a ferrimagnet. The structure of magnetite is shown in the fig. 11.

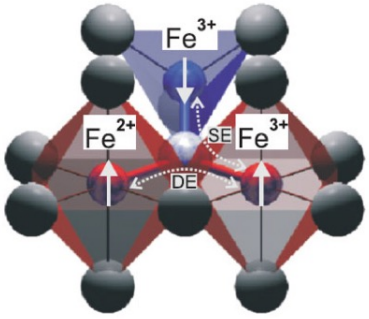

Figure 11: Crystallographic and magnetic structure of Fe_3O_4. Showing tetrahedrally (in blue) and octahedrally (in red), coordinated Fe atoms. The spheres around iron atoms are oxigen atoms. The moment on one of the Fe atom is coupled antiferromagnetically via superexchange (SE) to another Fe atom of the same valency and ferromagnetically via double exchange (DE) to a Fe atom of different valency. Adopted from [13].

For transition metals, like Fe, the orbital magnetic moment almost disappears and the magnetic moment comes mostly from the spin of unpaired electrons in its d-shell. However, the remaining small orbital moment couples to the electron spin(spin-orbit coupling) and creates magnetic anisotropy. Fe_3O_4 has cubic anisotropic with four magnetic easy-axis along the $< 111 >$ directions. This kind of cubic anisotropy is shown in fig. 12. Magnetite is magnetically soft and magnetic field above 100 mT is enough to magnetize the system in any direction. Thus, differences in magnetization dependent on the mutual orientation of the external field and the magnetic easy-axis should only be observed at low fields.

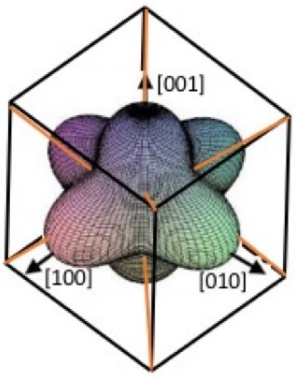

Figure 12: Cubic anisotropy represented with 4 easy axis along the diagonals of the cube($<$ 111 $>$ directions) marked in orange. The $< 100 >$ directions are the hard axis. Figure adapted from [11]

3 Experiment

3.1 Spark Discharge Technique

Calle Preger made the samples using this technique. Spark Discharge Generation (SDG) is an aerosol-based technique [14] used to generate the nanoparticles used in this study. A diagram of the process can be seen in fig. 13 (a). It consists of two metallic rods made up of the material from which the nanoparticles will be generated, here Fe. The rods are separated by a small gap, and a repeated spark discharges between the two, evaporating material which is transported away from the ablation zone by a carrier gas. Here, the carrier gas is nitrogen, but due to small amounts of oxygen in the system, the particles oxidize. The agglomerates that are formed in the electrode chamber are then neutralized to obtain a known charge distribution. The particles are selected by size with a Differential Mobility Analyzer (DMA) and transported through a furnace that reshapes them, with another DMA located after the tube furnace. Then the particles are guided to a substrate using an electric field (d). In this experiment, to maximize the signal to background, the nanoparticles were deposited onto a quartz substrate with a weak diamagnetic response.

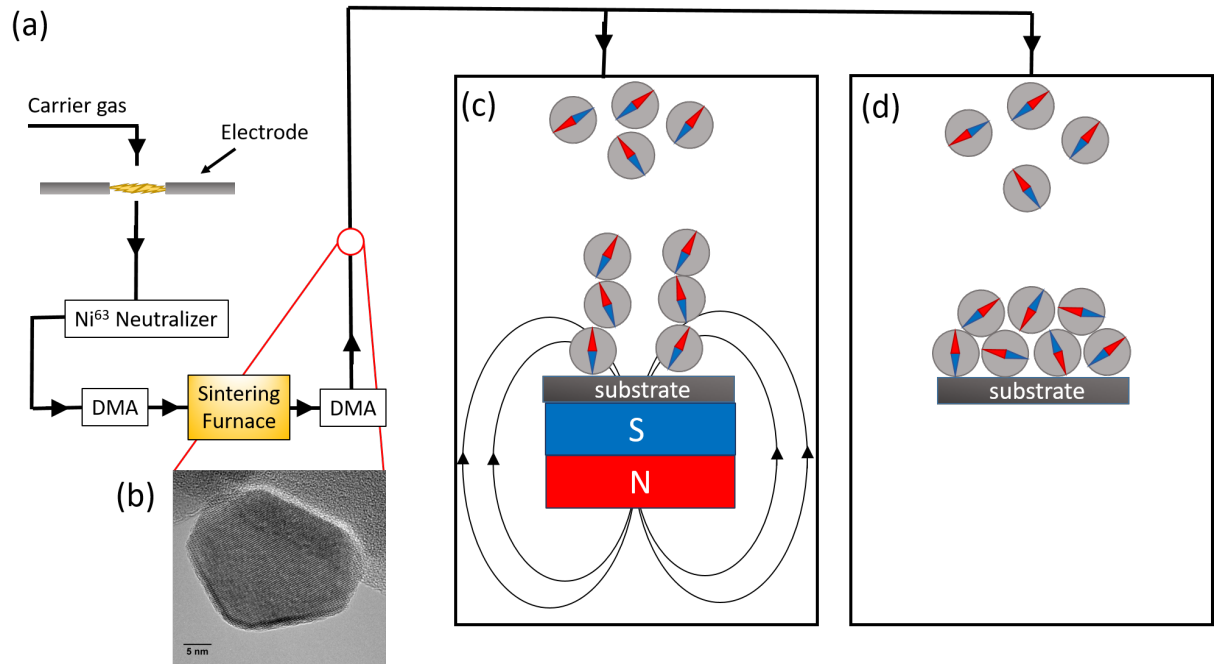

Figure 13: Figure showing in: (a) The schematics of SDG, (b) a Fe_3O_4 particle of 50 nm in diameter, (c) the fabrication of a NW sample with an applied magnetic field, (d) the fabrication of a NP sample without magnetic field. The compass needles indicate the crystallographic direction of the magnetic easy-axis for a uniaxial anisotropic system.

The nanoparticles start to self-assemble into one-dimensional structures as seen in fig. 1 when a magnetic field is applied together with the electric field. The formation of the NWs can be understood in a simple picture where the magnetic field magnetizes the nanoparticles in the gas phase before they reach the substrate, thus creating tiny "bar magnets" that are attracted to each other. The goal of this project is to study the magnetic response of 50 nm Fe_3O_4 nanoparticles deposited with and without a magnetic field. In the latter case, the nanoparticles will have a random crystallographic orientation and thus a random orientation of their magnetic easy-axis which defines the direction along which the magnetic moment of the particles have the lowest energy. If instead the particles are deposited in an applied magnetic field, it is expected that they will align their easy-axis out-of-plane,

3.2 SQUID measurement

The magnetic measurements were performed by a magnetometer using a Superconducting Quantum Interference Device (SQUID) as a magnetic sensor. Superconductivity is a state which occurs when some materials are at very low temperatures. The electrons couple to each other and become Cooper pairs. Cooper pairs act like bosons; particles that have integer spin and do not obey the Pauli exclusion principle. This means that the majority of the Cooper pairs occupy the same lowest energy state and are described with a single wavefunction. Since this state describes a measurable macroscopic property, the superconducting current, the corresponding wavefunction is sometimes referred to as a "macroscopic" wavefunction. The SQUID consists of a superconducting ring with two Josephson junctions, as shown in fig. 14. The superconducting current I, described by the "macroscopic" wavefunction φ, is split up along the two paths a and b ($I = I_a + I_b$), and then recombines again. As the wavefunctions φ_a and φ_b travel along the paths a and b, they experience a phase shift depending on the magnetic flux (here from the sample) threading the ring. When the two currents recombine, they experience constructive interference when the total magnetic flux Φ threading the ring is $\Phi = n\Phi_0$ where n is an integer and Φ_0 is the flux quanta which amounts to $\Phi_0 = 2 \cdot 10^{-15}\mathrm{Tm}^2$. Since the wavefunctions describe the macroscopic supercurrent across the SQUID loop, it will also vary with a periodicity given by the flux quanta. Variations in the supercurrent are determined by measuring the voltage across the SQUID circuit. The SQUID is thus an ultra-sensitive flux to voltage converter. [15]

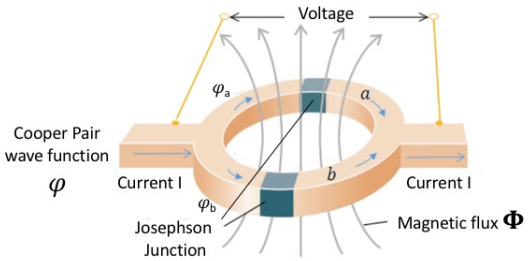

Figure 14: Part of the SQUID with two Josephson junction in a loop, figure adapted from [15].

4 Data and Discussion

The results of the experiment are presented here. The measurements are performed at two different temperatures to interpret a possible temperature dependent magnetic characterization. The difference between the two samples is the ordering of the particles. The particles have the same size and the same composition. But the average orientation of the easy-axis with respect to the applied magnetic field and possibly dipole-dipole interaction could differ. The magnetic deposition should result in the alignment of the crystallographic $< 111 >$ directions (the magnetic easy-axis) in the NW sample. For the NP sample, the deposition was performed without a magnetic field, and there should be no preferred orientation of the magnetic easy-axis. Starting with "as produced" non-magnetized samples, it could be expected that the initial magnetization would differ at low fields for the two systems. A model of the two samples is shown in fig. 15. It should be noted that the model depicts the simpler picture of uniaxial anisotropy whereas the present samples have cubic anisotropy with four magnetic-easy-axis and thus three additional "compass needles."

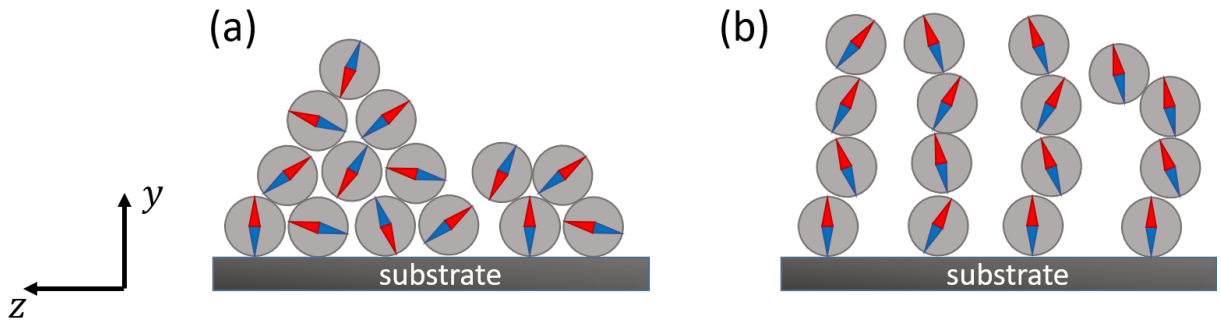

Figure 15: Model of the samples, showing in (a) a NP arrangement with random staking of particles and a ordered staking in NW (b). The compass needles indicate the crystallographic direction of the magnetic easy-axis for a uniaxial anisotropic system. It should be noted that the present systems have three additional magnetic easy-axis. The magnetic field is applied along the z-direction

4.1 Magnetization curves

The first result from the SQUID that is presented is the initial magnetization, also called the virgin curve. Starting from a demagnetized state and no applied magnetic. It slowly increases the applied field while measuring the magnetic moment of the sample up to 0.2 T then decreasing the magnetic field back to zero. The direction of the applied field is along the Z-direction, perpendicular to the direction of growth of the NW as seen in fig. 15. We did this measurement at two different temperatures, 300 K and 1.8 K, using liquid helium to lower the temperature. The results, shown in fig. 16 are normalized to the saturation magnetization at 7T obtained from a later measurement, see fig. 19. From fig. 16a it can be seen that the slopes and shape of the curves at 300 K are similar for the two systems, but with slightly higher magnetization for the NP at 0.2 T, and remanent magnetization for the NW sample. The similar magnetization behavior of the two systems at 300 K could be due to the softness of Fe_3O_4. Considering that the particles are about 25 nm smaller than the critical diameter for single-domain, the thermal energies could facilitate the magnetization to the extent that the alignment of the easy-axis has little effect on the response of the NW system. Still, there is an increase of about 10% in the remanent magnetization of the NWs.

To perform the same measurement at 1.8 K, we first had to demagnetize the sample. This was done by oscillating the magnetic field around zero at the maximum temperature of the system (400 K). The magnetization measurement at 1.8 K is shown in fig. 16 (b). At lower temperatures, it is harder to magnetize the samples since there are less thermal energies to help with overcoming the anisotropy barrier and it is expected that the orientation of the easy-axis will play a larger role. At 1.8 K we see a more significant difference

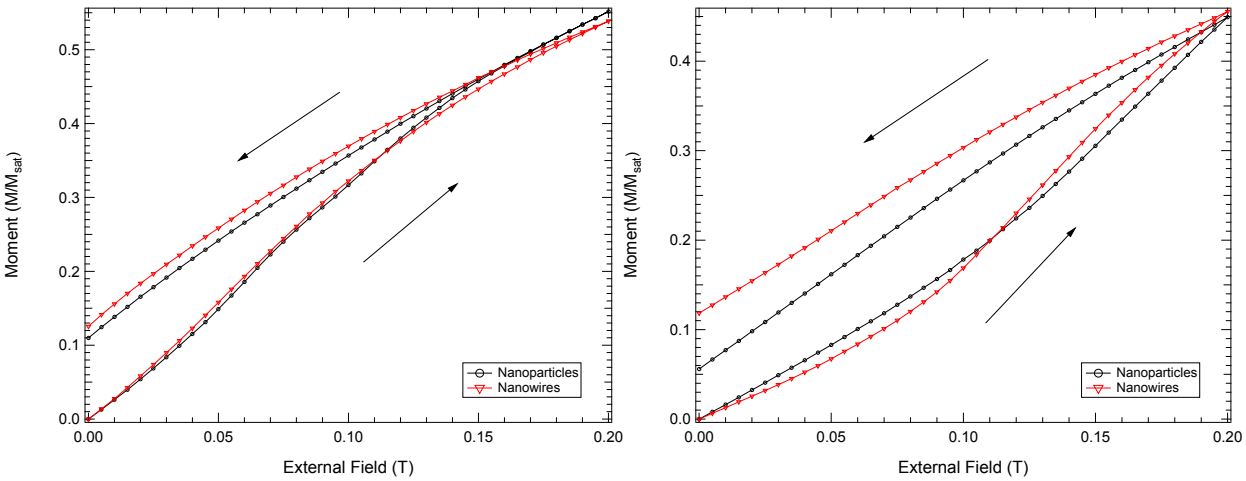

(a) (b)

Figure 16: Figure showing the magnetization curves from of the 2 samples, NW(red/triangular) and NP(black/circular), at 300 K (a) and 1.8 K (b).. The arrow indicates the field sweep direction.

between the two systems compared to room temperature. Initially, it is more difficult to magnetize the NW sample. This could be understood in the simplified picture of uniaxial nanoparticles where the easy-axis along the NWs should be close to perpendicular to the applied magnetic field. At around 0.1 T there's a change in slope, which is more notable for the ordered sample. As the field is increased above ~ 0.1 T, the slope of the two curves become similar. Bulk Fe_3O_4 can be magnetized in any direction at fields above 0.1 T, and it is therefore not surprising that the largest difference between the two samples is observed at field below ~ 0.1 T. As the field is decreased to zero again, the remanent magnetization is now two times higher for the NWs compared to the NP sample. It is also interesting to note that the remanent magnetization is more or less the same for the NWs, independent on the temperature. For both temperatures, the results show remanent magnetization, which tells us that indeed the samples are not super-paramagnetic. This is to be expected since the average size of the particles is 50 nm, our particles should be single-domain but not SPM. The critical diameter for SPM is around 10 nm and for single domain is 76 nm, according to the article [12].

The second result from the SQUID measurement is a magnetization curve that presents hysteresis, as already seen in fig. 5 hysteresis determines the magnetic characteristics of a material. By comparing the two samples, we can detect differences that were caused by the fabrication procedure. The measurement was taken starting at a high magnetic field, 7 T, and lowering the field to -7 T, then increasing the field to 7 T again. The displayed data has been normalized to the saturated magnetization at 7 T of each of the samples to be able to compare the two samples directly. Graph (b) has needed an error treatment that can be followed in section 6.3.

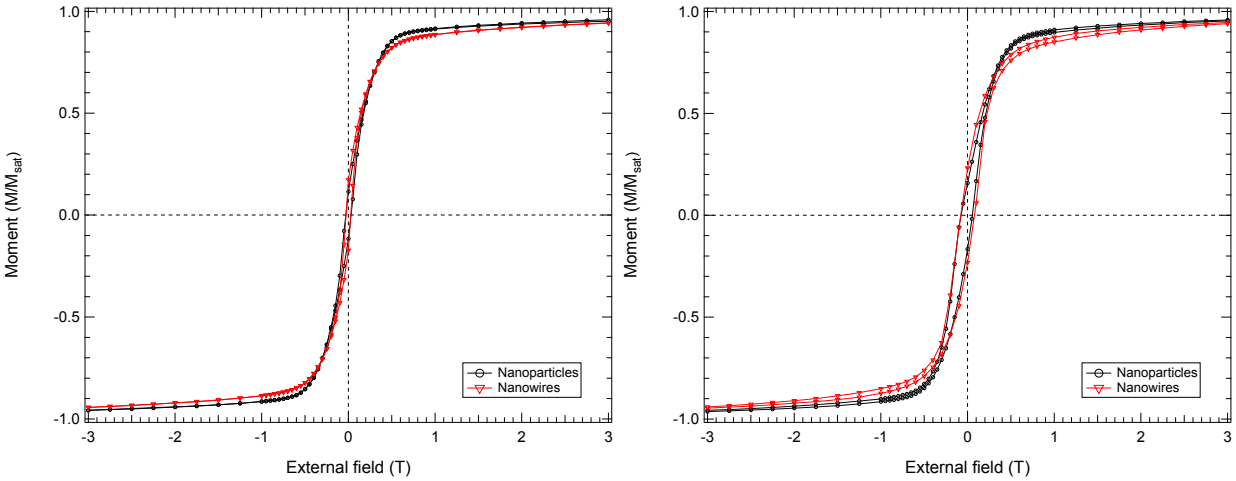

Figure 17: Magnetization curves recorded from NW(red/triangular) and NP(black/circular), at 300 K (a) and 1.8 K (b).

In fig. 17 the hysteresis curve is shown from 3 T to −3 T. The shapes of the magnetization curves are different. In fig. 18 we have performed a zoom of the center area to make a better analysis of the data. The most noticeable difference is the $\sim$ 50% increased remanent magnetization of the NW sample. The result from the Stoner-Wohlfarth model gives a different ratio for M_r/M_{sat} for an ordered sample and a randomly ordered. For the NW sample M_r/M_{sat} is more significant than the NP sample for both temperatures. The SW model also predicts that an ordered sample has a larger coercive field, but it happens to be the same for both samples. Based on the SW model, the increased M_r/M_{sat} ratio indicates that there is an alignment of the magnetic easy-axis in the NW sample. However, one should keep in mind that this model is a large oversimplification of the present system. In the SW model, it is assumed that the nanoparticles have uniaxial anisotropy, whereas the Fe_3O_4 has four easy-axis directed along the $< 111 >$ directions. However, if the magnetic deposition aligns one of the $< 111 >$ directions out-of-plane (y-direction in fig. 15), the rest of the easy-axis would also be ordered but along different directions. This means that the NW sample should still be more ordered than the NP sample. It is surprising that no difference in the coercive field is observed. For both systems, a coercivity of $\sim$ 30 mT observed at 300 K which is about twice as large as reported in [12] for similar sizes. The reported coercivity of Fe oxide nanoparticles in the literature varies from 30 to 44 mT[16], and the observed value is consistent with Fe_3O_4, possibly mixed with Fe_2O_3 nanoparticles.

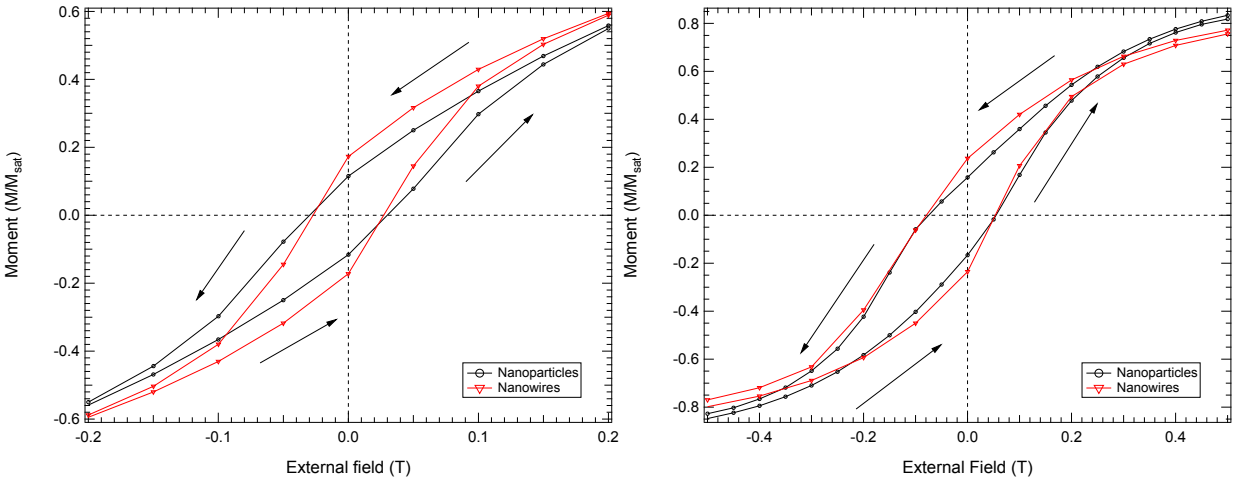

(a) (b)

Figure 18: Figure of 2 samples, NW(red/triangular) and NP(black/circular), showing the differences in remanent magnetizaiton and coercive field between the two hysterisis for fig. 17 in a zoomed area, a) 300 K and b) 1.8 K. The arrow indicates the field's sweep direction.

5 Conclusion and Outlook

Knowing that this experiment is part of a bigger project is important also to step back and realize the usefulness of the spark discharge technique. SDG is a useful technique which self-assembles tailored samples cheap and easily. In second instance, it is demonstrated that a magnetometer equipped with a SQUID detects the magnetic signal from these samples. What was discovered is that the ordering of the nanoparticles in NW structures results in a different response compared to the randomly oriented NP. Being this said, the results are not conclusive: Firstly I would repeat the hysteresis measurement at 1.8 K for the NW sample that since we got an error in the measurement. Because of the order dependent nature of the sample, an angle-dependent analysis is recommended. It would be interesting to try different sizes, and, especially, different materials. Also, an analysis considering the cubic anisotropy nature of the sample is required for a better understanding of the behavior of the angle dependence.

The magnetization curve reveals the response of the material under external magnetic field at 1.8 K and 300 K. It is clear that the system is temperature dependent, and when the system is at ambient temperature, the differences are less noticeable. The samples appear to behave similarly to a ferromagnet, so super-paramagnetism is discarded at ambient temperatures for these sizes. Temperature-dependent measurements could provide additional information about the sample. Therefore the temperature dependent measurement where the variable is the temperature, and the field is stable is recommended. Lastly, we do not know the exact structure of the samples. Therefore a scanning electron microscope

(SEM) measurement would provide a direct visual of the sample that would facilitate an understanding of the structure itself.

References

[1] S. Ekeroth et al. "catalytic nanotruss structures realized by magnetic self-assembly in pulsed plasma". *Nano Letters (Print)*, 18(5), 2018.

[2] Jie et al Yin. "nio/con porous nanowires as efficient bifunctional catalysts for zn–air batteries". *ACS Nano*, 11(2):2275–2283, 2017. PMID: 28195696.

[3] Jia et al Liu. "electromagnetic property and tunable microwave absorption of 3d nets from nickel chains at elevated temperature". *ACS Applied Materials & Interfaces*, 8(34):22615–22622, 2016. PMID: 27509241.

[4] Xuefeng et al Zhang. "high-magnetization feco nanochains with ultrathin interfacial gaps for broadband electromagnetic wave absorption at gigahertz". *ACS Applied Materials & Interfaces*, 8(5):3494–3498, 2016. PMID: 26775668.

[5] H. Zeng et al. "exchange-coupled nanocomposite magnets by nanoparticle self-assembly". *Nature*, 420:395, 2002.

[6] E.C. Stoner and E.P. Wohlfarth. "a mechanism of magnetic hysteresis in heterogeneous alloys". *Phil. Tran. Roy. Soc. Lond.*, 240(826), 1948.

[7] Andrey Geim. "everyone's magnetism". *Physics Today*, 51(9):36, 1998.

[8] A. Aharoni. *"Introduction to the Theory of Ferromagnetism"*. International Series of Monographs on Physics. Clarendon Press, 2000.

[9] Joan Estelrich, Elvira Escribano, Josep Queralt, and Maria Busquets. "iron oxide nanoparticles for magnetically-guided and magnetically-responsive drug delivery". *International Journal of Molecular Sciences*, 16:8070–8101, 04 2015.

[10] modified by Joshua Halpern https://chem.libretexts.org. "3d representation of orbitals", 2017.

[11] Günther Bayreuther. "magnetic anisotropy", 2011.

[12] Li Qing, Kartikowati Christina W., Horie Shinji, Ogi Takashi, Iwaki Toru, and Okuyama Kikuo. "correlation between particle size/domain structure and magnetic properties of highly crystalline fe3o4 nanoparticles". *Scientific Reports*, 7(1):1, 2017.

[13] Joachim Stohr and Hans Christoph Siegmann. *"Magnetism. From Fundamentals to Nanoscale Dynamics"*. Springer-Verlag Berlin Heidelberg, 2006.

[14] Maria Messing. "the advantages of spark discharge generation for manufacturing of nanoparticles with tailored properties". *Journal of Green Engineering*, 5:83–96, 01 2016.

[15] John Clarke. "squids". *Scientific American*, 271(2):46–53, 1994.

[16] C Baker, S Ismat Shah, and S.K Hasanain. Magnetic behavior of iron and iron-oxide nanoparticle/polymer composites. *Journal of Magnetism and Magnetic Materials*, 280(2-3):412 – 418, 2004.

6 Appendix

6.1 Appendix 1: Full field range Hysteresis and raw data

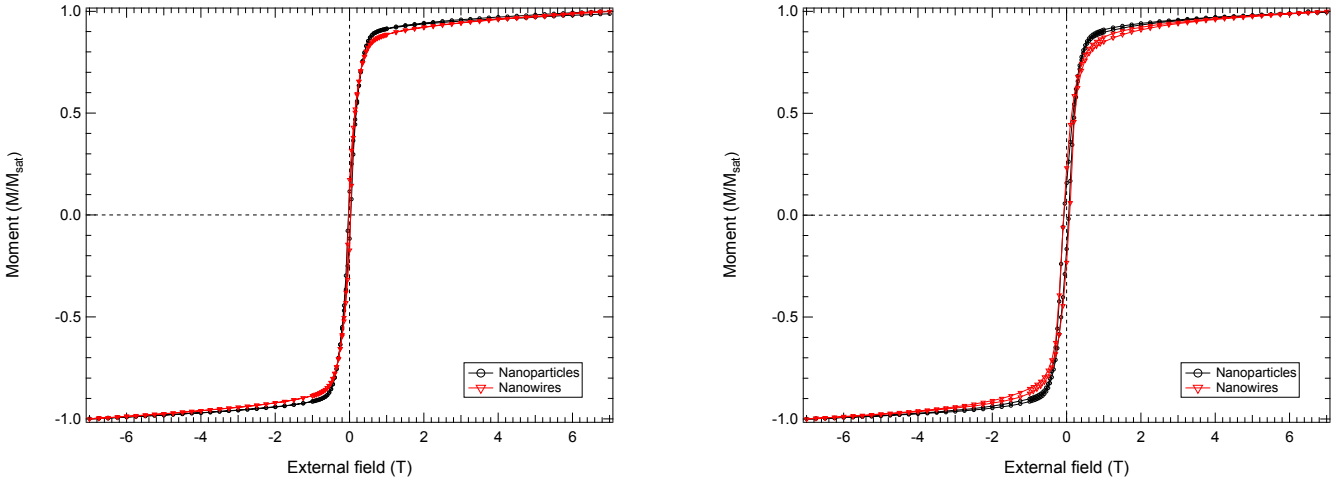

Figure 19: Figure of 2 samples, NW(red/triangular) and NP(black/circular), showing the full magnetization curve from -5 T to 5 T, at 300 K at the left and 1.8 K at the right, a lower saturation magnetization for the nanowire structure is noticed.

6.2 Appendix 2: Transfer of samples into the SQUID

Description of the facility:

The measurement was done the 19th to the 25th of March. The facility lies in University of Zurich Campus Irchel. In the facility of physics. The primary use of the lab is the SQUID although it had some other devices on use. In figure 20 there can be seen a view of our workstation.

Figure 20: Image of the facility where the measurement was taken to the left the computer with some code can be seen behind it the SQUID and behind the SQUID there is the table from figure 22 and figure 23 to the right there's another desk where we were analysing the output data.

In fig. 21 we see the center of the SQUID. There is a cylindrical structure where the sample is introduced with a movable yellow marker which gives information about the movement of the sample. On top of the white tubular structure, there is a black part which acts as a lid and seals the interior while measuring. If the chamber is purged and the pressure inside is equal to the ambient pressure, the lid can be opened, and the sample arm with the sample holder attached to it can be introduced.

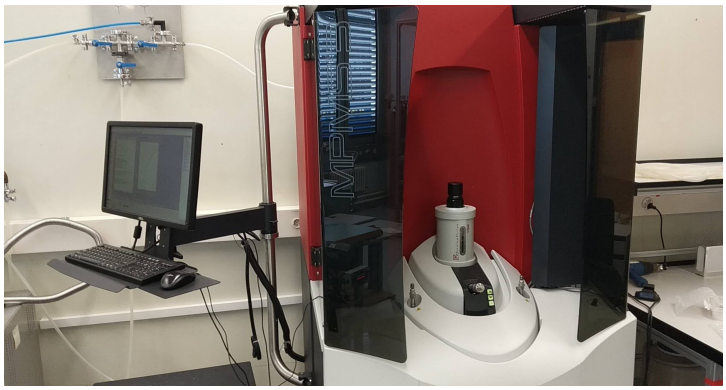

Figure 21: Image if the front view of the SQUID, computer to the right. On the left the SQUID can be seen, elegant design with glass doors, behind which the sample arms are kept

The samples are in a quartz plate, which is fragile by itself, so we glued it to a robust quartz holder. The quartz holder needs a treatment to get rid of the previous sample and of the impurities that may have attached to it. By treating the holder with Ethanol, as can be seen in fig. 22, we make sure it stays clean.

Figure 22: Image of the tools used and the quartz sample holder under treatment.

Once the holder is clean, the procedure to paste can be seen in fig. 23, using varnish to fix the sample to the holder and then wrapping the connection in Kapton tape, which remains stable across a wide range of temperatures.

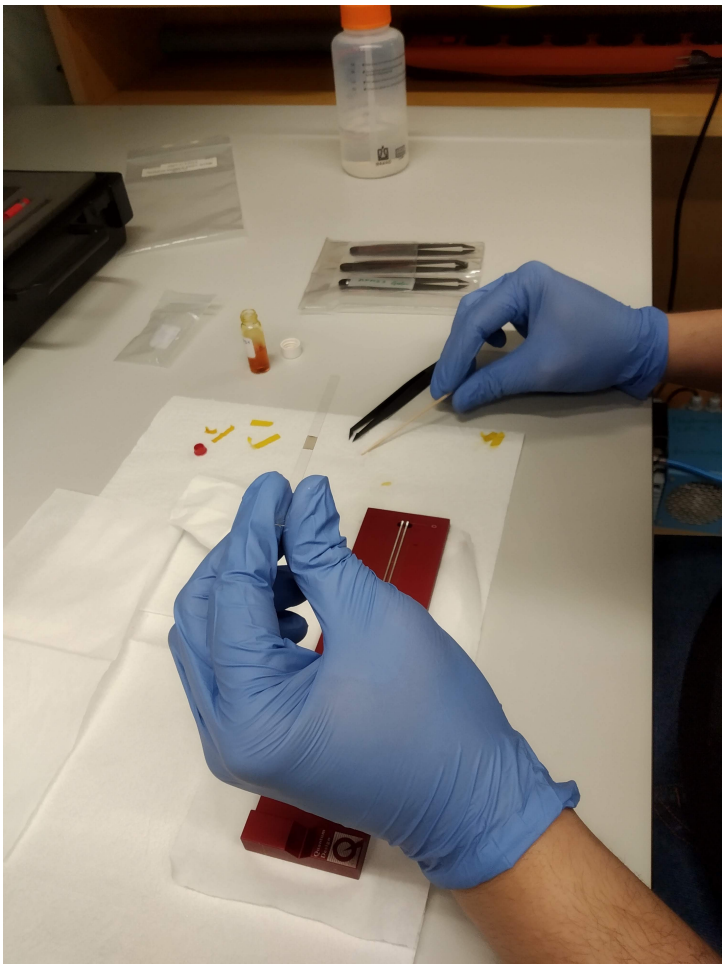

Figure 23: Image showing the sample which being glued to the sample holder.

To glue the sample to the quartz sample holder.

6.3 Appendix 3: Error treatment

Data error treatment of the experiment for the NW sample at 1.8 K. As it can be seen in fig. 24 there appeared an offset at 1.4 T.

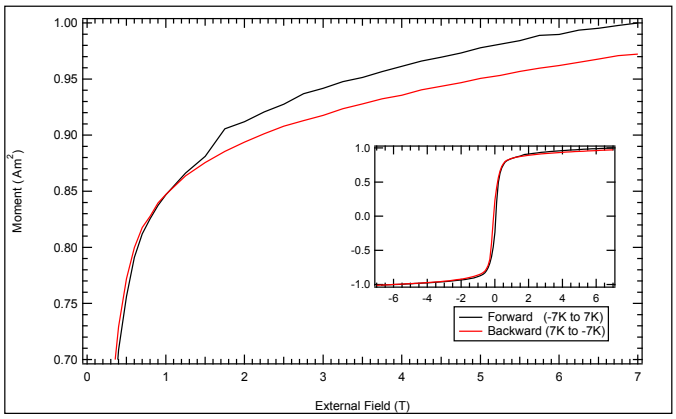

Figure 24: Figure showing an error in the measurement of the full hysteresis at 1.8 K. Measurement started at 7 T and descended following the red line until −7 T. Then the field was increased again, and the measurements followed the black line. It can be seen a lack of symmetry around 1 T and a noticeable jump around 1.7 T.

In order to present fig. 17b and fig. 18b a data correction needed to be done. To do it we found support in the fact that the hysteresis is symmetric around its center. Therefore, the curve can be divided into four segments as seen in fig. 25. The segments BP, BN and FN, are the original data. But FP is the same data as in BN after performing an inversion as $x = -x$, $y = -y$.

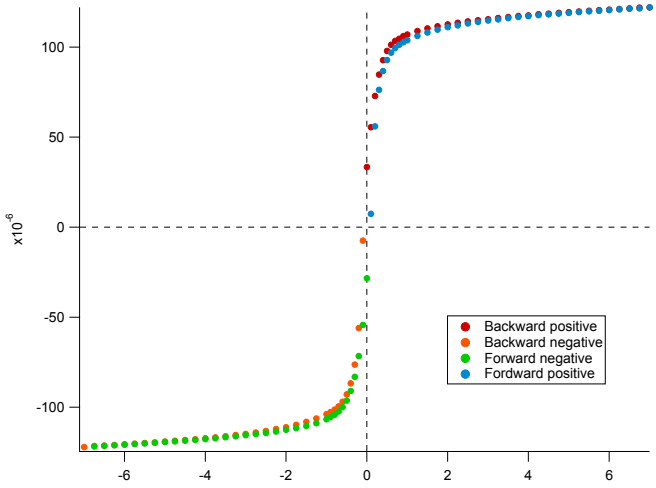

Figure 25: Figure showing the raw data after a first change. Separating the wave in four parts, backward sweep from positive to negative applied external field, and forward sweep from negative to positive applied external field. The different segments are referred to in the text by their initials Ex: Forward negative FN.